Low-Complexity PRF-Agile Radar Maneuvering Target Detection via ANS-ATRT-VEM

Jiawei Wang, Yong Gao

***Abstract*—This paper presents a robust and low-complexity method for maneuvering target detection in pulse repetition frequency agile radar systems. We introduce a new paradigm—a conditional dependency-based sequential decoupling framework. In contrast to conventional paradigms that either fragment the problem (divide-and-conquer) or confront it with exhaustive search (global optimization), our framework explicitly leverages the inherent hierarchical dependencies within the signal model. It establishes a strictly ordered processing chain: the ambiguity number search first compensates for the dominant range migration and achieves envelope alignment directly in the time domain. This, in turn, enables the augmented time-reversal transform to separate velocity and acceleration phases analytically. Finally, with the decoupled signal structure, the virtual echo modeling synthesizes an expanded virtual array aperture from very few pulses. This sequential dependency transforms a high-dimensional, coupled estimation problem into a series of tractable low-dimensional sub-tasks. The framework is supported by comprehensive theoretical analysis, including closed-form detection probability in the virtual domain, verification of its constant-false-alarm-rate property, and derivation of the Cramér–Rao lower bound under non-uniform sampling. Simulations under low signal-to-noise ratio and severely limited pulse conditions demonstrate that the proposed method significantly outperforms state-of-the-art techniques in estimation accuracy, computational efficiency, and robustness, providing a principled and practical solution for high-speed maneuvering target detection in agile radar systems.**

***Index Terms*—Pulse repetition frequency-agile radar, maneuvering target detection, sequential decoupling, virtual array.**

I. Introduction

PULSE radar systems are widely deployed in modern sensing applications such as surveillance, remote sensing, and autonomous navigation, owing to their capability for long-range detection and high-resolution parameter estimation. The pursuit of higher estimation accuracy—whether in radar cross-section characterization [1] or in the fundamental resolution limits imposed by waveform design [2]—has long driven advances in both theory and system design. In this context, pulse repetition frequency (PRF)-agile radar (PAR) has emerged as an important system-level evolution of conventional non-agile radar (NAR). By introducing pulse-to-pulse PRF variation, PAR offers enhanced operational flexibility, improved anti-jamming robustness, and better echo fidelity under low signal-to-noise ratio (SNR) conditions. However, the task of tracking highly maneuvering targets over long-time coherent integration (LTCI) intervals exposes several intrinsic challenges in PAR systems. These challenges are not independent—they exhibit a hierarchical coupling structure: PRF-induced sparsity provides the backdrop against which range migration (RM), Doppler ambiguity, and model mismatch manifest and interact. Specifically [3]–[5]:

1) PRF agility introduces randomness and sparsity in the slow-time domain, invalidating conventional LTCI techniques that rely on uniform sampling assumptions and fast Fourier transform (FFT)–based processing.
2) Target-induced RM, including first-order RM (FRM) caused by high target velocity and second-order RM (SRM), namely Doppler frequency migration (DFM), caused by target acceleration, leads to range cell misalignment and nonlinear phase modulation, thereby severely degrading coherent integration (CI) gain.
3) When the target Doppler frequency exceeds the PRF, Doppler aliasing occurs, resulting in velocity ambiguity and reduced accuracy of motion-parameter estimation.
4) Time-varying target motion over long observation intervals often causes model mismatch, especially for abrupt or nonlinear maneuvers, which limits the effectiveness of fixed-model-based processing methods.

Extensive research efforts in recent years have been devoted to mitigating these challenges to achieve accurate motion-parameter estimation and effective LTCI in PAR systems.

First, to address the non-uniform slow-time sampling induced by PRF agility, the non-uniform fast Fourier transform (NUFFT) has been applied for spectral estimation on irregular sampling grids [6]. Building upon this, the Radon-NUFFT method [7] incorporates the Radon transform to enhance CI performance. Moreover, combining the Radon transform with the non-uniform fractional Fourier transform (NUFrFT) has demonstrated improved motion-parameter estimation for complex maneuvering targets [8]. While these methods improve motion-parameter estimation, their high computational complexity hinders real-time applications.

Second, RMs due to target motion substantially degrade CI performance. For FRM induced by constant velocity, methods such as the Radon Fourier transform (RFT) [9]–[11] and the keystone transform (KT) [12]–[14] are widely employed. However, these techniques are ineffective in compensating for DFM caused by acceleration. To jointly address FRM and SRM, advanced methods such as the Radon-fractional Fourier transform (RFRFT) [15], Radon-linear canonical transform (RLCT) [16], and Radon-Lv's distribution (RLVD) [17] have been proposed. These methods can correct nonlinear phase distortions, but multiple domain transformations and interpolations increase computational load and may introduce

Jiawei Wang and Yong Gao are with the College of Electronics and Information Engineering, Sichuan University, Chengdu 610041, China (e-mail: wangjw626@163.com; gaoyong@scu.edu.cn).

approximation errors, affecting parameter estimation accuracy. Separately, the generalized RFT (GRFT) [18], [19] addresses similar problems through a powerful but computationally intensive multi-dimensional parameter search, which has also motivated significant research into more efficient implementations [20].

Third, velocity ambiguity remains a persistent issue. Subsampling in the fast-time domain yields incorrect radial-velocity estimation. Li et al. [21] proposed a folding-factor compensation method in the fast-time frequency domain to estimate the ambiguity number. However, this approach relies on multiple Fourier and inverse Fourier transforms as well as prior motion knowledge, which may introduce cumulative approximation errors and reduced robustness. To enhance ambiguity resolution, a robust ambiguity number search method based on the Chinese remainder theorem (CRT) was introduced in [22] to reduce the search dimensionality, although large ambiguity ranges still impose a considerable computational burden.

Fourth, LTCI is essential for accurate motion-parameter estimation under low SNR. However, real target motion often deviates significantly from fixed models over extended observation intervals, leading to model mismatch in conventional processing—a challenge that is not only pertinent to detection but also a central concern in tracking theory [23]Traditional short-time time-frequency analysis techniques—such as the short-time Fourier transform (STFT) [24] and the short-time fractional Fourier transform (STFRFT) [25]—are typically applied heuristically by segmenting the signal for piecewise analysis. To better accommodate non-stationary motion dynamics, the short-time GRFT (STGRFT) [26] was developed specifically for radar applications, enabling simultaneous compensation of RMs under time-varying motion. Nevertheless, these methods remain computationally intensive and require scenario-specific tuning, limiting practical implementation.

Although the aforementioned studies have achieved progress from different perspectives, the problem of maneuvering target parameter estimation in PAR systems has not yet been comprehensively resolved. A fundamental difficulty lies in the fact that non-uniform sampling, RM, Doppler ambiguity, and acceleration-induced nonlinearities are inherently and hierarchically coupled in the signal model. Existing methods predominantly follow either a "divide-and-conquer" paradigm or a "global optimization paradigm", neither of which fully exploits this coupling structure.

In the "divide-and-conquer" approach, the challenges are addressed through serial processing modules (e.g., handling non-uniform sampling, followed by RM compensation and then ambiguity resolution). While this reduces the complexity of individual modules, it neglects the strong coupling between them. For instance, velocity ambiguity and FRM are linearly intertwined in the slow-time phase model, and accurate acceleration estimation critically depends on precise velocity compensation. Such fragmented processing inevitably leads to error propagation and suboptimal performance, while the overall computational cost remains significant. In contrast, "global optimization" approaches, exemplified by the GRFT and its variants, tackle parameter coupling through exhaustive high-dimensional searches. While theoretically optimal, their computational complexity scales exponentially with the number of motion parameters (range, velocity, and acceleration), succumbing to the "curse of dimensionality" and hindering real-time implementation. This underscores a fundamental bottleneck in applying search-based strategies to strongly coupled problems. Therefore, a new paradigm capable of systematically addressing this intrinsic coupling while maintaining low computational complexity is urgently needed.

A promising alternative is to leverage virtual array theory in the slow-time domain. Our earlier study [27] pioneered this concept for PAR by constructing virtual echoes, providing an initial foundation. However, its practical application to maneuvering targets was constrained by three principal limitations: 1) a zero-acceleration model, which fails to capture realistic target dynamics; 2) an unresolved velocity ambiguity, requiring external processing; and 3) the neglect of intra-cell envelope shifts under sparse pulses. Critically, these shortcomings all originate from an inability to address the underlying coupling among motion parameters, which distorts the virtual array manifold. To resolve this core issue, this paper puts forward a fundamental insight: the effective application of virtual array theory in this context constitutes a targeted "signal reconstruction" goal, not a directly applicable starting point. Achieving this goal strictly depends on two prerequisites that must be met sequentially: (i) envelope alignment to establish a valid slow-time spatial analogy; and (ii) phase decoupling to obtain a linear, single-parameter phase manifold.

Driven by this insight, this paper proposes a novel conditional dependency-based sequential decoupling paradigm. Unlike approaches that treat the challenges independently, this paradigm explicitly exploits the inherent hierarchical dependencies within the signal model to construct a strictly ordered processing chain: the ambiguity number search (ANS) first compensates for the dominant RM to achieve envelope alignment (Condition i); this enables the Augmented time-reversal transform (ATRT) to separate velocity and acceleration phases in the time domain (Condition ii); finally, given the decoupled signal structure, virtual echo modeling (VEM) synthesizes an expanded virtual aperture for ultimate performance enhancement. Consequently, a high-dimensional, nonlinear joint estimation problem is transformed into a sequence of structured low-dimensional sub-problems, instantiated as the ANS-ATRT-VEM algorithmic chain. The main contributions of this paper are summarized as follows:

1) Paradigm contribution: a Conditional Dependency-Based Sequential Decoupling framework is proposed, offering a novel methodology for systematically tackling coupled parameter estimation in PAR systems.
2) Algorithmic and foundational contribution: the ANS-ATRT-VEM processing chain is developed with strict internal dependency. This clarifies, for the first time, that: (a) ANS is the necessary enabler for time-domain envelope alignment and disambiguation; (b) ATRT is the key mechanism enabling direct time-domain phase decoupling; and (c) VEM is not merely a processing step but the realization of the core concept: the synthesis of a slow-time virtual aperture from very few pulses, which is the ultimate goal of the proposed paradigm.

3) Validation contribution: comprehensive theoretical analysis, and theoretical verification of the constant false alarm rate (CFAR) property in the virtual echo domain, together with extensive simulations and ablation studies, conclusively demonstrates the novel method's superior estimation accuracy, computational efficiency, and robustness.

The remainder of this paper is organized as follows. Section II introduces the signal model and preprocessing for maneuvering targets with acceleration. Section III details the proposed low-complexity CI method for both single- and multi-target scenarios, supported by theoretical analysis. Section IV presents the computational-complexity analysis and simulation-based performance evaluation. Section V concludes the paper and outlines directions for future research. Additional theoretical derivations supporting the proposed method are provided in the Appendix A.

Notations : Throughout this paper, lower-case (upper-case) bold characters represent vectors (matrices). $(\cdot)^{\mathrm{T}}$ and $(\cdot)^{\mathrm{H}}$ denote the transpose and conjugate transpose operation of a matrix or a vector, respectively. $\mathrm{vec}(\cdot)$ denotes the vectorization, square root operation, and the determinant of a matrix. $\mathrm{E}(\cdot)$ is the statistical expectation operator.

II. Signal Model and Pre-processing

A. Signal Model

Assuming that M pulses are transmitted within a coherent processing interval (CPI), with each pulse employing linear frequency modulation (LFM) for intra-pulse modulation, the transmitted signal model can be expressed as follows:

$$S_t(\hat{t}, t_m) = \mathrm{rect}(\hat{t}/T_p)\exp[j\pi\gamma\hat{t}^2 + j2\pi f_c(\hat{t}+t_m)] \quad (1)$$

where $\mathrm{rect}(x) = \begin{cases} 1, & |x| \le 0.5 \\ 0, & else \end{cases}$, $\hat{t}$ is the fast time, T_p is the pulse duration, $\gamma = B/T_p$ is the frequency modulation rate, B is the bandwidth, and f_c is the carrier frequency. The slow time t_m is defined as:

$$t_m = p(m)T_r, m = -\frac{M-1}{2}, \cdots, 0, \cdots, \frac{M-1}{2} \quad (2)$$

where T_r is the reference pulse repetition interval (PRI), and $p(m)$ is a real-valued increasing sequence satisfying $p(\hat{m}) = -p(m)$ with $\hat{m} = M - m + 1$ being the symmetric index of m about zero, which encodes the PRF agility pattern of PAR.

B. Pre-processing

Considering (1) as the radar transmitted pulse, assume there are G maneuvering targets. The parameters r_g, v_g, and a_g describe the range, velocity, and acceleration of the gth target (where $g = 1, \cdots, G$), respectively. Positive values for velocity and acceleration indicate that the target is moving in the direction of the radar. After applying pulse compression (PC), the corresponding echo signals are given by:

$$S_r(\hat{t}, t_m) = \sum_{g=1}^{G} \tilde{A}_{m,g}(\hat{t})\exp(-j2\pi f_c\tau_{m,g}) \quad (3)$$

$$\tilde{A}_{m,g}(\hat{t}) = A_{1,g}\mathrm{sinc}[\pi B(\hat{t}-\tau_{m,g})] \quad (4)$$

where $\tau_{m,g} = 2(r_g - v_g t_m - a_g t_m^2)/c$ represents the time delay of the gth target's echo corresponding to the mth transmitted pulse, where c denotes the speed of light. The parameter $A_{1,g}$ indicates the amplitude of the pulse-compressed echo from the gth target, and $\mathrm{sinc}(x) = \sin(\pi x)/(\pi x)$ is the sinc function.

III. Detection Target via ANS-ATRT-VEM

The proposed method constructs a sequential mapping from the raw echo space $\mathcal{E}$ to a virtual array space $\mathcal{V}$:

$$\mathcal{E} \xrightarrow{\mathcal{F}_{ANS}} \mathcal{E}_{aligned} \xrightarrow{\mathcal{F}_{ATRT}} \mathcal{E}_{decoupled} \xrightarrow{\mathcal{F}_{VEM}} \mathcal{V} \quad (5)$$

where each mapping is well-defined only after the previous one, enforcing a hierarchical dependency that decouples range, velocity, and acceleration without multidimensional search. Here $\mathcal{F}$ denotes the transformation, with the subscript specifying the operation.

A. ANS

In PAR systems, the Doppler frequency of a fast-moving target is inevitably aliased, leading to severe velocity ambiguity and RM across pulses. Specifically, the true target velocity can be decomposed as:

$$v_g = N_{bg}v_b + v_{0g} \quad (6)$$

where $v_b = c/(2f_cT_r)$ denotes the blind velocity, $N_{bg} \in \mathbb{Z}$ is the Doppler ambiguity number, and v_{0g} represents the unambiguous velocity component satisfying $|v_{0g}| < v_b/2$.

Substituting (6) into the pulse-compressed echo model in (3), the envelope term can be rewritten as:

$$\tilde{A}_{m,g} = A_{1,g}\mathrm{sinc}\{\pi B[\hat{t} - 2(r_g - N_{bg}v_b t_m)/c - \tilde{\tau}_{m,g}\} \quad (7)$$

where $\tilde{\tau}_{m,g} = 2(-v_{0g}t_m - a_g t_m^2)/c$.

Key observation: for high-speed targets, the dominant RM is governed by the ambiguity-related term $2N_{bg}v_b t_m/c$, whereas $\tilde{\tau}_{m,g}$ corresponds to a residual intra-cell displacement. In practice, this residual term satisfies:

$$\tilde{\tau}_{m,g} \ll 2(-N_{bg}v_b t_m)/c \quad (8)$$

and is typically much smaller than the width of a single range resolution cell defined by the sinc mainlobe.

As a result, the echo signal in (3) can be approximated as:

$$S_r(\hat{t}, t_m) \approx \sum_{g=1}^{G} B_{m,g}(\hat{t})\exp(-j2\pi f_c\tau_{m,g}) \quad (9)$$

where $B_{m,g}(\hat{t}) = A_{1,g}\mathrm{sinc}\{\pi B[\hat{t} - 2(r_g - N_{bg}v_b t_m)/c]\}$.

(9) reveals that the ambiguity number N_{bg} directly determines the dominant range walk of the target across pulses. Importantly, once N_{bg} is correctly estimated, the ambiguity-induced RM can be removed in the time domain, aligning the sinc envelopes of the target echoes without requiring frequency-domain interpolation or resampling.

Since the blind velocity v_b is known a priori, the ambiguity number N_{bg} takes values from a finite integer set. The search range for N_{bg} is determined by the maximum plausible radial

velocity of the target, denoted as v_{max} . Specifically, N_{bg} is searched over the integer set:

$$\mathcal{N} \in \left\{ \left\lfloor -\frac{v_{\max}}{v_b} \right\rfloor, \ldots, \left\lceil \frac{v_{\max}}{v_b} \right\rceil \right\} \tag{10}$$

This ensures that all physically possible velocities are covered while maintaining computational efficiency. With the search range thus defined, N_{bg} can be efficiently estimated via a low-complexity one-dimensional (1-D) integer search over $\mathcal{N}$. Unlike conventional velocity unfolding methods that operate in the Doppler-frequency domain, the proposed ANS explicitly exploits the time-domain structure of the pulse-compressed sinc envelope, making it particularly suitable as a pre-processing step for subsequent time-domain CI.

Let $\hat{N}_{bg}$ denote the estimated ambiguity number of the gth target. After ambiguity compensation, the echo signal evaluated at $\hat{t} = 2r_g/c$ can be expressed as:

$$\begin{aligned}
\tilde{S}_{r,1}(\hat{t}, t_m) &= [C_1(\hat{t}) + \textstyle\sum_{g=2}^{G} D_{m,1}(\hat{t})] \exp(-j2\pi f_c \tau_{m,1}) \\
&\vdots \\
\tilde{S}_{r,g}(\hat{t}, t_m) &= [C_g(\hat{t}) + \textstyle\sum_{i\neq g}^{G} D_{m,i}(\hat{t})] \exp(-j2\pi f_c \tau_{m,g}) \\
&\vdots \\
\tilde{S}_{r,G}(\hat{t}, t_m) &= [C_G(\hat{t}) + \textstyle\sum_{g=1}^{G-1} D_{m,G}(\hat{t})] \exp(-j2\pi f_c \tau_{m,G})
\end{aligned} \tag{11}$$

where $C_g(\hat{t}) = A_{1,g}\mathrm{sinc}[\pi B(\hat{t} - 2r_g/c)]$, and

$$D_{m,i}(\hat{t}) = A_{1,i}\mathrm{sinc}\{\pi B[\hat{t} - 2(r_g - N_{bg} v_b t_m + N_{bi} v_b t_m)/c]\} \approx 0 \tag{12}$$

where $\hat{t} = 2r_g/c$.

After ambiguity compensation, each target produces a dominant peak at its corresponding range cell, enabling simultaneous velocity disambiguation, RM correction, and target enumeration. This process is computationally efficient. Although extracting all G targets may require up to G iterations in the worst case, targets sharing the same ambiguity number can be processed jointly within a single iteration—significantly reducing the overall cost.

The search for N_{bg} itself is adaptive and data-driven: for each candidate integer N, we perform envelope compensation followed by slow-time coherent integration; the correct N generates a distinct integrated peak, while incorrect candidates yield defocused energy. Therefore, the search terminates naturally upon peak detection, eliminating reliance on a predefined (and often inaccurate) maximum velocity prior. This strategy enhances robustness, particularly for targets exhibiting extreme radial dynamics (e.g., ballistic or hypervelocity objects).

B. ATRT

The time-reversal transform (TRT) has been extensively studied as an effective tool for maneuvering target detection, where parameter decoupling is typically achieved through frequency-domain formulations [28]. Existing TRT-based approaches are inherently developed within the fast-time frequency domain, in which motion-induced phase terms are explicitly separated and processed.

In this work, rather than reformulating conventional TRT, we introduce an ATRT enabled by the preceding ANS stage. Specifically, ANS compensates the dominant ambiguity-induced RM and restores a slow-time-aligned envelope structure across pulses. This structural regularization gives rise to a previously unexplored property: the existence of a symmetric slow-time pair whose fast-time envelopes are equivalent up to deterministic phase terms.

Based on this restored symmetry, the echo corresponding to the symmetric slow-time index $\hat{m}$ can be expressed as:

$$\tilde{S}_{r,g}(\hat{t}, t_{\hat{m}}) = C_g(\hat{t}) \exp\big(-j2\pi f_c \tau_{\hat{m},g}\big). \tag{13}$$

It is emphasized that such a representation does not hold in general prior to ambiguity compensation, as the fast-time envelopes associated with different pulses are misaligned due to motion-induced migration.

By multiplying (11) with the conjugate of (13), a time-reversal-induced product is obtained as

$$\begin{aligned}
X_{1,g}(\hat{t}, t_m) &= \tilde{S}_{r,g}(\hat{t}, t_m)\, \mathrm{conj}\big(\tilde{S}_{r,g}(\hat{t}, t_{\hat{m}})\big) \\
&= C_g^2(\hat{t}) \exp\big(j8\pi f_c v_g t_m / c\big),
\end{aligned} \tag{14}$$

where the quadratic motion-induced phase terms are inherently canceled through the symmetric slow-time structure, leaving a pure linear phase term associated with the target velocity.

Similarly, by directly multiplying (11) with (13), another complementary product is obtained as

$$\begin{aligned}
X_{2,g}(\hat{t}, t_m) &= \tilde{S}_{r,g}(\hat{t}, t_m) \tilde{S}_{r,g}(\hat{t}, t_{\hat{m}}) \\
&= C_g^2(\hat{t}) \exp\big[-j8\pi f_c (r_g - a_g t_m^2)/c\big],
\end{aligned} \tag{15}$$

in which the velocity-dependent phase term is eliminated, while the acceleration-induced quadratic phase term is preserved.

Therefore, ATRT establishes a structured time-reversal mechanism in the slow-time domain, enabling an intrinsic separation of velocity and acceleration information without resorting to multidimensional parameter searching. This transform is not a direct variant of conventional TRT, but rather a new instantiation made possible by the envelope-aligned structure produced by ANS.

C. VEM

1) Virtual echo construction: The structured outputs generated by ATRT in (14) and (15) exhibit a key property: after ambiguity compensation and symmetric slow-time pairing, the slow-time dimension admits a deterministic exponential manifold analogous to that encountered in array signal processing. This observation enables a principled reinterpretation of the ATRT outputs within a virtual array framework, leading to the proposed VEM.

Specifically, by collecting the ATRT outputs across range cells, (14) and (15) can be reformulated into the following array-consistent models:

$$\begin{aligned}
\hat{\mathbf{Y}}_{1,g} &= [\boldsymbol{x}_{1,g}(1), \cdots, \boldsymbol{x}_{1,g}(n), \cdots, \boldsymbol{x}_{1,g}(N)] \\
&= \boldsymbol{\varphi}_{1,g} \boldsymbol{a}_{1,g},
\end{aligned} \tag{16}$$

$$\begin{aligned}
\mathbf{Y}_{2,g} &= [\boldsymbol{x}_{2,g}(1), \cdots, \boldsymbol{x}_{2,g}(n), \cdots, \boldsymbol{x}_{2,g}(N)] \\
&= \boldsymbol{\varphi}_{2,g} \boldsymbol{a}_{2,g},
\end{aligned} \tag{17}$$

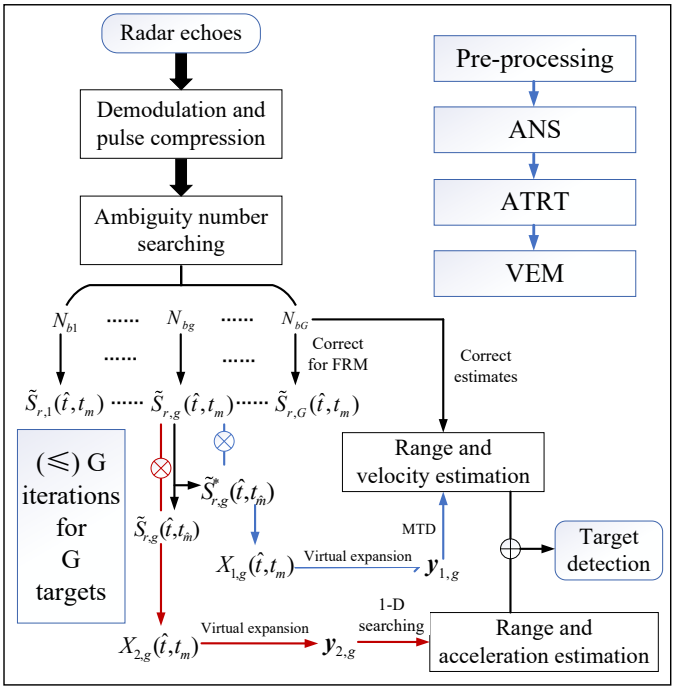

Fig. 1. Flowchart of the proposed method.

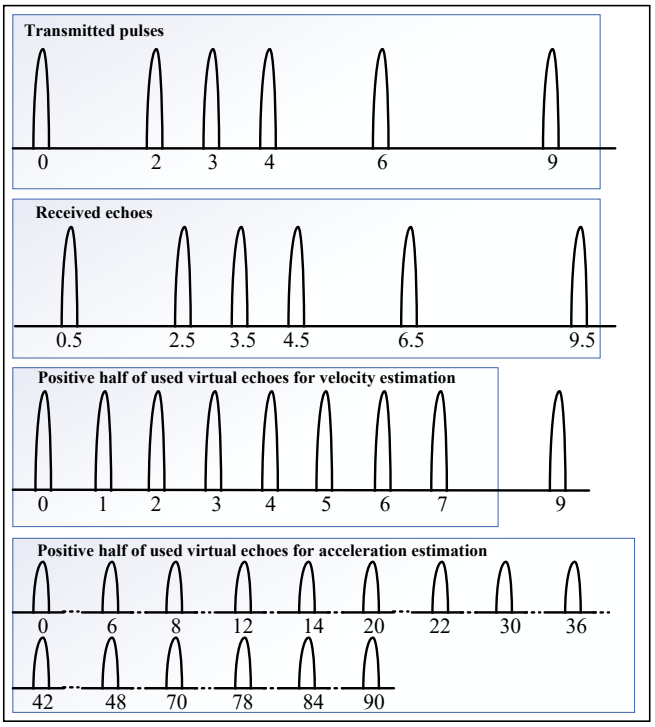

Fig. 2. Virtual echoes generated based on the ACA-$(2,3,1)_2$ configuration (for clarity, only the positive half-axis is shown, as only half of the physical echoes remain available for VEM after ATRT processing).

where N denotes the number of range cells and $\boldsymbol{x}_{i,g}(n) = [X_{i,g}(\hat{t}_n, t_1), \cdots, X_{i,g}(\hat{t}_n, t_M)]^{\mathrm{T}}$ for $i = 1, 2$. The corresponding steering vectors are given by

$$\boldsymbol{\varphi}_{1,g} = [\exp(j8\pi f_c v_g t_1/c), \cdots, \exp(j8\pi f_c v_g t_{(M+1)/2}/c)]^{\mathrm{T}},$$

$$\boldsymbol{\varphi}_{2,g} = [\exp(j8\pi f_c a_g t_1^2/c), \cdots, \exp(j8\pi f_c a_g t_{(M+1)/2}^2/c)]^{\mathrm{T}},$$

while $\boldsymbol{a}_{1,g} = [C_g^2(\hat{t}_1), \cdots, C_g^2(\hat{t}_N)]$ and $\boldsymbol{a}_{2,g} = \boldsymbol{a}_{1,g}\exp(-j8\pi f_c r_g/c)$ collect the range-dependent amplitudes.

It is emphasized that the array-consistent structures in (16)–(17) do not exist in the original echo domain. They emerge only after ATRT suppresses velocity–acceleration coupling and restores a coherent slow-time manifold, which is a prerequisite for any meaningful array interpretation.

To further exploit this structure, the covariance matrixs (CMs) of the ATRT outputs are constructed as

$$\mathbf{R}_{1,g}(n) = \mathrm{E}[\boldsymbol{x}_{1,g}(n)\boldsymbol{x}_{1,g}^{\mathrm{H}}(n)] = \boldsymbol{\varphi}_{1,g}H_{1,g}(n)\boldsymbol{\varphi}_{1,g}^{\mathrm{H}}, \quad (18)$$

$$\mathbf{R}_{2,g}(n) = \mathrm{E}[\boldsymbol{x}_{2,g}(n)\boldsymbol{x}_{2,g}^{\mathrm{H}}(n)] = \boldsymbol{\varphi}_{2,g}H_{2,g}(n)\boldsymbol{\varphi}_{2,g}^{\mathrm{H}}, \quad (19)$$

where $H_{1,g}(n) = C_g^4(\hat{t}_n)$ and $H_{2,g}(n) = H_{1,g}\exp(-j16\pi f_c r_g/c)$.

By vectorizing (18) and (19) and removing redundant phase terms, the following virtual echo representations are obtained:

$$\begin{aligned}\hat{\boldsymbol{y}}_{1,g}(n) &= \mathrm{vec}(\mathbf{R}_{1,g}(n)) \\ &\rightarrow \tilde{\boldsymbol{y}}_{1,g}(n) = \boldsymbol{u}_{1,g}H_{1,g}(n) \in \mathbb{C}^{U_1\times 1},\end{aligned} \quad (20)$$

$$\begin{aligned}\boldsymbol{y}_{2,g}(n) &= \mathrm{vec}(\mathbf{R}_{2,g}(n)) \\ &\rightarrow \boldsymbol{y}_{2,g}(n) = \boldsymbol{u}_{2,g}H_{2,g}(n) \in \mathbb{C}^{U_2\times 1},\end{aligned} \quad (21)$$

where $\boldsymbol{u}_{1,g} = [\exp(j8\pi f_c v_g q_1^1), \cdots, \exp(j8\pi f_c v_g q_u^1), \cdots, \exp(j8\pi f_c v_g q_{U_1}^1)]^{\mathrm{T}}$ and $\boldsymbol{u}_{2,g} = [\exp(j8\pi f_c a_g q_1^2), \cdots, \exp(j8\pi f_c a_g q_u^2), \cdots, \exp(j8\pi f_c a_g q_{U_2}^2)]^{\mathrm{T}}$. Here, $q_u^1 \in \mathbb{U}_1 = \{t_i - t_j | 1 \le i, j \le (M+1)/2\}$ and $q_u^2 \in \mathbb{U}_2 = \{t_i^2 - t_j^2 | 1 \le i, j \le (M+1)/2\}$ represent the first- and second-order slow-time difference sets, respectively, which are used to construct virtual echoes within the difference co-array (DC) framework.

As illustrated in Fig. 2, the virtual echoes generated by the proposed difference-set construction significantly expand the effective aperture, even though only half of the physical pulses remain available after ATRT processing.

The continuous segment of $\boldsymbol{y}_{1,g}(n)$ is then extracted from $\tilde{\boldsymbol{y}}_{1,g}(n)$ and assembled into $\mathbf{Y}_{1,g} = [\boldsymbol{y}_{1,g}(1), \cdots, \boldsymbol{y}_{1,g}(N)]^{\mathrm{T}}$, which serves as the virtual echo matrix for range and velocity estimation using conventional moving target detection (MTD).

Once the target range is determined, the corresponding column of $\mathbf{Y}_{2,g}$ is selected and processed via (19) and (21) to construct $\boldsymbol{y}_{2,g}(i)$, from which the acceleration a_g is then estimated via a 1-D search over a physically plausible range $[a_{min}, a_{max}]$, determined by prior knowledge of the target type and its expected maneuverability.

Finally, the estimated motion parameters are substituted into (6) for signal compensation. A localized quadratic refinement around the estimated ambiguity number N_{bg} is further performed to enhance ambiguity resolution accuracy, particularly in scenarios involving long observation intervals or unambiguous velocities close to the blind velocity.

2) Sparse linear array (SLA): SLA have attracted considerable attention in array signal processing because of their ability to provide high degrees of freedom (DoFs) with relatively few physical elements. By constructing the DC framework from received signals, these arrays synthesize an expanded virtual aperture, thereby markedly improving resolution and

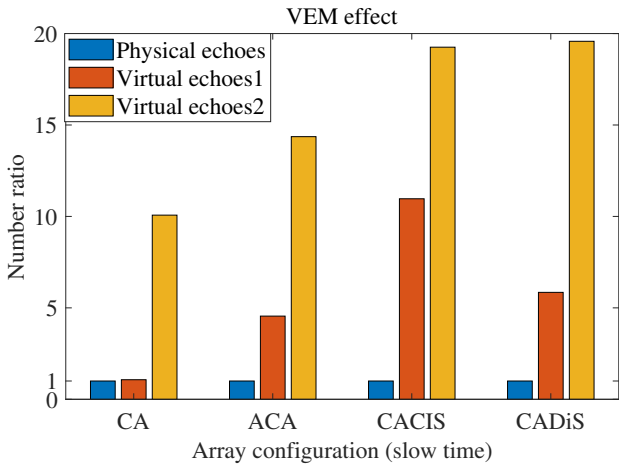

Fig. 3. Expansion effect based on VEM.

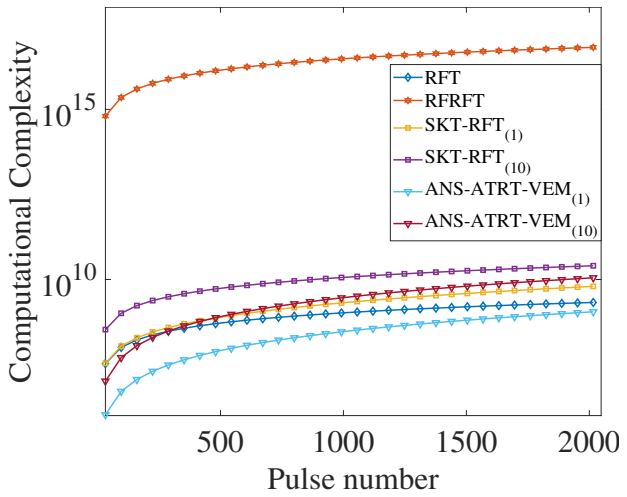

Fig. 4. Computational complexity.

estimation performance while keeping hardware complexity and cost low. This advantage is especially crucial in PAR systems, where generating a large number of virtual echoes from a limited set of transmitted pulses is essential.

For clarity, four representative SLA configurations considered in the subsequent study are introduced: the co-prime array (CA) [29], the augmented CA (ACA) [30], the CA with compressed inter-element spacing (CACIS) [31], and the CA with displaced subarrays (CADiS) [31]. Each configuration provides distinct advantages in aperture extension, DoFs enhancement, and redundancy reduction, making them particularly well suited for virtual echo construction within the DC framework.

$$\mathbb{P}_1 = \{pQd|0 \le p \le P-1\} \cup \{qPd|0 \le q \le Q-1\} \quad (22)$$

$$\mathbb{P}_2 = \{pQd|0 \le p \le 2P-1\} \cup \{qPd|0 \le q \le Q-1\} \quad (23)$$

$$\mathbb{P}_3 = \{pQd|0 \le p \le P-1\} \cup \{q\tilde{P}d|0 \le q \le Q-1\} \quad (24)$$

$$\mathbb{P}_4 = \{q\tilde{P}d|0 \le q \le Q-1\} \cup \{(pQ+J)d|0 \le p \le P-2\} \quad (25)$$

TABLE I
MOTION PARAMETERS OF RADAR AND TARGET

Parameters	NAR	PAR
Carrier frequency	0.15GHz	0.15GHz
Bandwidth	2MHz	2MHz
Sample frequency	10MHz	10MHz
PRF	500Hz	*
Pulse duration	5us	5us
Number of pulses	512	65 [ACA-$(11,12,1)_2$]

* Basic PRF is set as 900Hz. Due to the random setting of slow time and varying pulse group numbers based on specific requirements, the PRI cannot be directly specified, but it is approximately 500 Hz.

	Range (km)	Velocity (m/s)	Acceleration (m/s^2)
Target A	100	2500	200
Target B	105	2600	150
Target C	100	1500	20

TABLE II
VIRTUAL ECHO EXPANSION EFFECT [29]

Slow time	M	N_{e1}
$(P,Q,d)_1$	$2(P+Q)-3$	$2(P+Q)-1$
$(P,Q,d)_2$	$2(2P+Q)-3$	$2P(Q+1)-1$
$(P,Q,\delta,d)_3$	$2(P+Q)-3$	$2Q(P-\tilde{P})-2\tilde{P}-1$
$(P,Q,\delta,d)_4$	$2(P+Q)-3$	$PQ-(\tilde{P}-1)(Q-2)+1$

*Unlike N_{e1}, a concise closed-form expression for N_{e2} has not yet been derived due to the increased complexity.

TABLE III
COMPARISON COMPUTATIONAL COMPLEXITIES

Methods	Mc
RFT	MNN_v
RFRFT	$8MNN_vN_aN_p + 2MNN_vN_aN_p\log_2 M$
SKT-RFT	$NM^2 + GN_vMN$
Proposed method	$MN + \tilde{G}N(M/2)^2 + G(M/2)^2 + \tilde{G}N(N_{e1}/2)\log_2(N_{e1}) + GN_{e2}N_a$

*Denote the number of searching transform order, searching velocity and searching acceleration by N_p, N_v and N_a.

where Z denotes integer set, P and Q are mutually prime integer, k and d are positive numbers. $P{=}\delta\tilde{P}$, δ is an integer between 2 and P, $J = \tilde{P}+Q$. For ease of use, the parameters of the above arrays are sequentially recorded as $(P,Q,d)_1$, $(P,Q,d)_2$, $(P,Q,\delta,d)_3$ and $(P,Q,\delta,d)_4$.

IV. SIMULATIONS

To rigorously assess the proposed method, simulation studies are presented from four perspectives: (1) the ability of the proposed VEM to synthesize substantially more echoes than the number of transmitted pulses; (2) a comparative evaluation of computational complexity against several conventional approaches; (3) performance under severely constrained pulse conditions, demonstrating the VEM's advantage in maintaining estimation accuracy; and (4) detection performance against widely used methods in both single- and multi-target scenarios.

A. Virtual Echo Expansion Enabled by VEM

The proposed method's echo expansion constitutes a key innovation and is validated across multiple array configurations. For a fair comparison, the number of virtual echoes—specifically, the continuous subset used for velocity

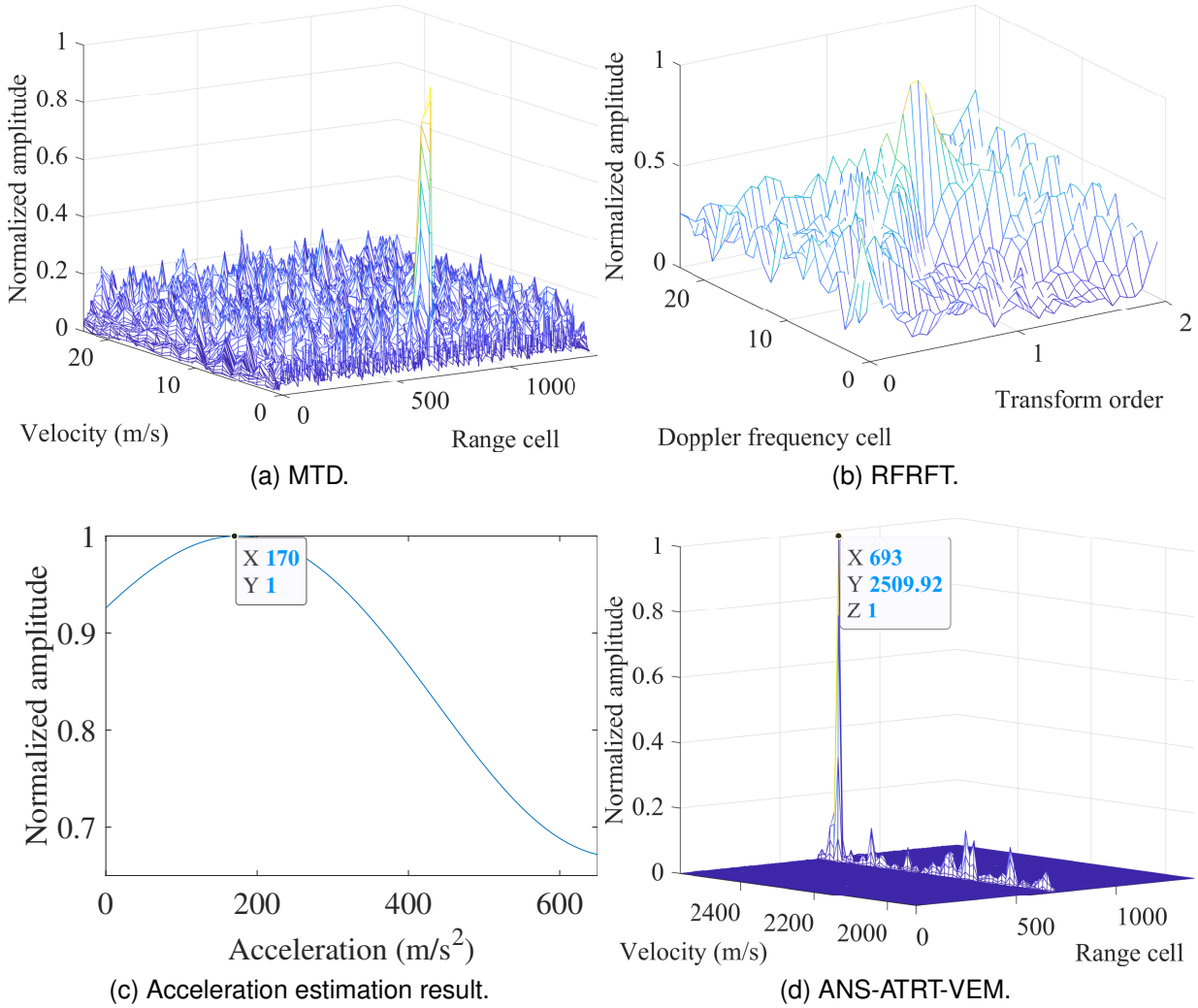

(a) MTD. (b) RFRFT. (c) Acceleration estimation result. (d) ANS-ATRT-VEM.

Fig. 5. CI for target A under extremely limited pulses (SNR=-5dB).

estimation and the complete set employed for acceleration estimation—is normalized by the number of physical echoes obtained under the same number of transmitted pulses.

It should be noted that the number of virtual echoes for velocity estimation, denoted as N_{e1}, admits a closed-form expression (as shown in Table II). In contrast, the number of virtual echoes for acceleration estimation, denoted as N_{e2}, exhibits a more complex pattern and does not admit a concise closed-form expression; only numerical examples can be provided for specific parameter sets.

In Fig. 3, for each of the four array structures, 20 experiments are conducted with varying initial numbers of physical echoes. For each structure, the figure shows the total ratio — i.e., the sum of virtual echoes divided by the sum of physical echoes across all 20 experiments — for velocity estimation and acceleration estimation, alongside the physical echo benchmark (fixed at 1).

As shown in Figs. 2 and 3 and Table II, the proposed method generally achieves at least a fivefold improvement compared with conventional approaches. Although this improvement is influenced by the initial slow-time configuration, it substantially reduces radar workload, facilitates real-time detection by decreasing the number of required transmitted pulses, and effectively mitigates RMs in LTCI scenarios.

B. Computational Complexity Analysis

To provide a fair comparison of computational complexity, the number of complex multiplications (Mc) and additions (Ac) is evaluated for the RFT [9]–[11], RFRFT [15], second-order KT-RFT (SKT-RFT) [32], and the proposed method.

The flowchart of ANS-ATRT-VEM is shown in Fig.1:

1) ANS: For each candidate ambiguity number N_{bg1}, apply row-wise time-delay compensation followed by coherent summation into a single vector for peak detection. The associated complexity is $N_s(M-1)N$ Ac.
2) ATRT: Two forms of row-wise symmetric multiplications yield $\hat{\mathbf{Y}}_{1,g}$ and $\mathbf{Y}_{2,g}$, requiring MN Mc.
3) VEM: For VEM1, the dominant complexity arises from computing the CM for each column of $\mathbf{Y}_{1,g}$, requiring $\tilde{G}N(M/2)^2$ Mc. For VEM2, the CM computation for one column of $\mathbf{Y}_{2,g}$ requires $G(M/2)^2$ Mc.

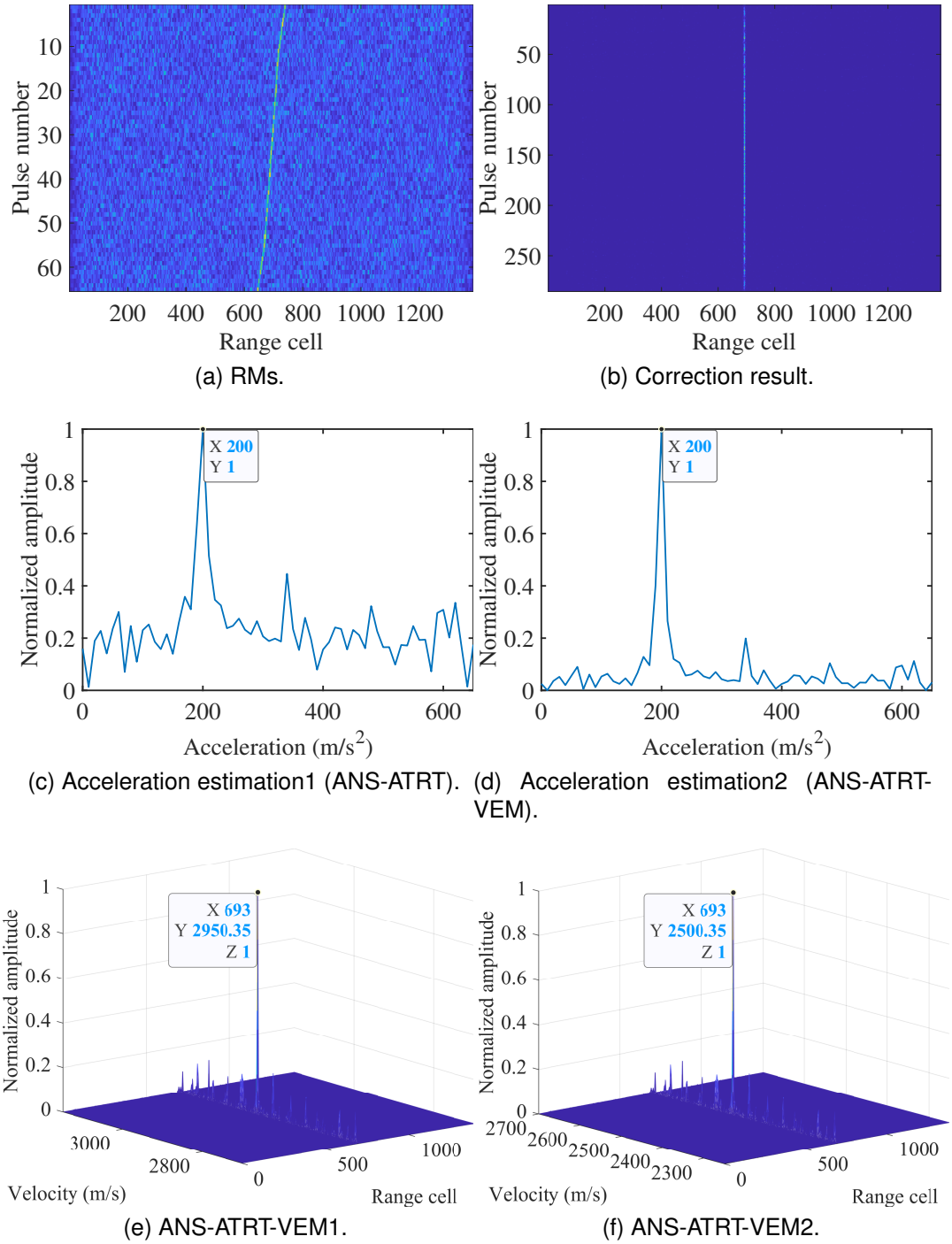

(a) RMs. (b) Correction result.

(c) Acceleration estimation1 (ANS-ATRT). (d) Acceleration estimation2 (ANS-ATRT-VEM).

(e) ANS-ATRT-VEM1. (f) ANS-ATRT-VEM2.

Fig. 6. CI for target A (SNR=-5dB).

4) Parameters estimation: For velocity estimation, apply FFT along the slow-time dimension of VEM1, with $\tilde{G}N(N_{e1}/2)\log_2 N_{e1}$ Mc and $\tilde{G}NN_{e1}\log_2 N_{e1}$ Ac. For acceleration estimation, conduct a 1-D search over VEM2, incurring $GN_{e2}N_a$ Mc and $G(N_{e2}-1)N_a$ Ac.
5) Ambiguity number refinement: Based on the estimated motion parameters, a local refinement of the ambiguity number is conducted to improve estimation precision. Owing to its confined search scope, the additional computational cost is minimal.

where N_s denotes the number of ANS candidates, and $\tilde{G}$ is the actual number of distinct ambiguity numbers associated with G targets. Thus, the overall complexity of ANS-ATRT-VEM can be expressed as: $MN+\tilde{G}N(M/2)^2+G(M/2)^2+\tilde{G}N(N_{e1}/2)\log_2(N_{e1})+GN_{e2}N_a$ Mc and $N_s(M-1)N+G(N_{e2}-1)N_a+\tilde{G}NN_{e1}\log_2(N_{e1})$ Ac.

Based on the results shown in Fig. 3 and Table II, the parameters are configured as $\tilde{G}=G$ and $N_{e1}=N_{e2}=5M$ to ensure a fair and consistent comparison. Since the number of targets directly influences the complexity of both SKT-RFT

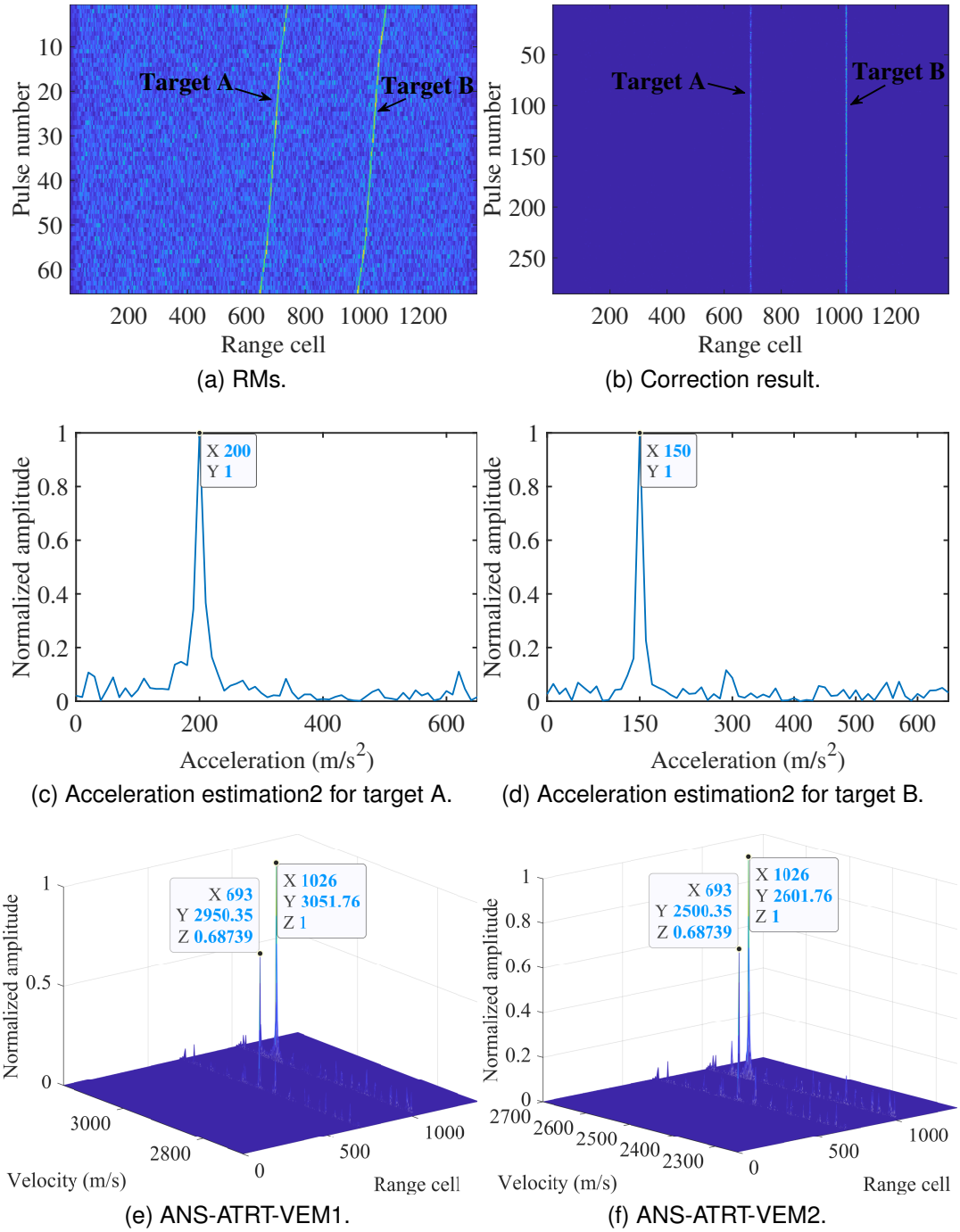

Fig. 7. CI for targets A and B (SNR=-5dB).

and the proposed method, simulations are carried out under two representative scenarios: a single target (ANS-ATRT-VEM$_{(1)}$) and ten targets (ANS-ATRT-VEM$_{(10)}$). To maintain uniformity, the configuration is set as $N_s = N_v = N_a = N_p = N$, while the number of transmitted pulses is varied from 32 to 2048, as shown in Fig. 4.

Among all evaluated methods, RFRFT exhibits by far the highest computational complexity. In contrast, the proposed ANS-ATRT-VEM achieves the lowest complexity in the single-target scenario and remains only marginally higher than RFT and SKT-RFT in the ten-target case (i.e., SKT-RFT$_{(10)}$). These findings confirm the computational efficiency of the proposed method, which mainly arises from its avoidance of computationally intensive multi-dimensional parameter searches—a primary source of computational complexity in conventional approaches.

It should also be noted that the above comparison assumes an equal number of transmitted pulses across all methods for computational complexity evaluation. In practice, however, the proposed method can operate with significantly fewer transmitted pulses by exploiting virtual echo generation. As a result, its practical computational complexity is anticipated

to be even lower than that shown in Fig. 4.

C. Performance under Extremely Limited Pulses

To validate that the proposed method maintains effective target detection performance by generating a substantial number of virtual echoes even under severely constrained pulse transmissions, an experiment was conducted using only 23 pulses configured as CACIS-$(6, 7, 3, 1)_3$. For a fair comparison, all radar parameters were kept consistent with those in Table I, except for the number of transmitted pulses.

The results illustrated in Figs. 5 highlight the following key observations:

1) Mitigation of RMs: Under reduced pulse conditions, RMs are substantially mitigated, as evidenced by the MTD results, demonstrating the method's robustness in tracking maneuvering targets with minimal pulse transmissions.
2) Virtual echo enhancement: Despite the shortened observation interval, the proposed method generates a sufficient number of virtual echoes to preserve high estimation accuracy, whereas conventional methods exhibit significant resolution degradation.
3) Acceleration estimation degradation: Acceleration estimation performance deteriorates under severely limited pulse numbers, resulting in considerable errors even when employing VEM.
4) Accurate initial ANS: The influence of target motion, as characterized in (8), becomes negligible due to the short detection time, thereby allowing the initial ANS to produce accurate estimates.

These findings underscore the method's capability to ensure reliable detection and parameter estimation even with very few transmitted pulses, primarily due to the effective generation of virtual echoes via VEM.

D. Target Detection Capability

This section assesses the detection and estimation performance of the proposed method via both single-trial experiments—including single- and multi-target scenarios—and Monte Carlo simulations based on the CFAR criterion, thereby validating its robustness under diverse operational conditions. The experimental parameters are summarized in Table I.

1) Single-Trial Experiments: This subsection investigates the estimation accuracy of the proposed method under both single-target and multi-target conditions. Key observations from Figs. 6 and 7 are summarized as follows:

1) The proposed method consistently detects and accurately estimates both single and multiple maneuvering targets, demonstrating robustness across a variety of target configurations and motion parameters.
2) Compared with the version without VEM (Fig. 6c), the VEM-integrated method (Fig. 6d) substantially enhances acceleration estimation accuracy. While both methods yield correct estimates, the VEM-enabled approach achieves higher resolution and more effectively suppresses spurious responses, particularly under low SNR conditions.

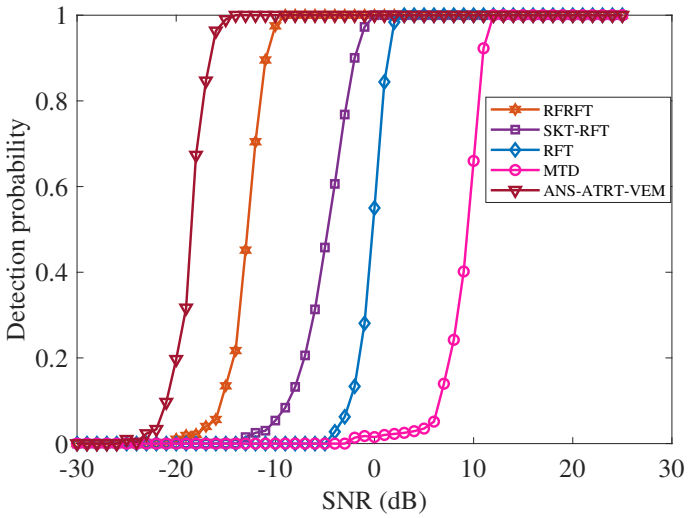

Fig. 8. Detection performance for target C (false alarm probability is set to 10^{-3}).

3) As the number of transmitted pulses increases, the extended observation interval amplifies RMs induced by target motion, occasionally causing minor deviations in the initial ANS results (Figs. 6e and 7e). These deviations, however, are effectively corrected by the second-stage refinement (Figs. 6f and 7f), ultimately producing highly accurate parameter estimates.

Collectively, these results demonstrate the method's capability to achieve high-precision parameter estimation even in complex and dynamically evolving target scenarios.

2) Detection Performance: To mitigate the randomness inherent in single-trial evaluations, a CFAR-based assessment comprising 1000 Monte Carlo trials is conducted across varying SNR conditions. For all compared methods, the false alarm probability is uniformly set to $P_{fa} = 10^{-3}$, with CFAR applied in their respective final detection domains to ensure statistical fairness.

As illustrated in Fig. 8, the proposed method consistently outperforms several representative methods, thereby demonstrating substantially enhanced target detection performance. This detection improvement is attributed to the enhanced integration gain achieved through virtual echo synthesis, which effectively increases the equivalent number of coherently integrated pulses. Beyond its superior detection capability, the method exhibits strong operational efficiency by requiring fewer transmitted pulses and incurring lower computational complexity. This efficiency arises from effectively eliminating the need for high-dimensional parameter searches while simultaneously transforming the physical PAR into a virtual NAR system. Such characteristics render the approach particularly well-suited for real-time implementation and deployment in resource-constrained, real-world target detection scenarios.

V. Conclusion

This study presents a low-complexity framework for detecting maneuvering targets and determining their motion

parameters in PAR systems. The proposed approach integrates three key components—ANS, ATRT, and VEM—to overcome the effects of slow-time randomness, RMs, and Doppler ambiguity that typically degrade parameter estimation accuracy in PAR systems. The ANS enables reliable estimation of the Doppler ambiguity number and ensures correct first-order range alignment directly in the time domain, while the ATRT provides accurate compensation of Doppler frequency migration without the need for multidimensional searches. Additionally, the VEM converts sparse PAR echoes into a uniform virtual observation structure, enhancing parameter estimation resolution with fewer transmitted pulses. A comprehensive set of simulations conducted under different motion patterns, SNR levels, and agility conditions confirms the effectiveness of the proposed framework. The results demonstrate consistent improvements in motion-parameter estimation accuracy, reduced integration-time requirements, and enhanced robustness to non-stationary target dynamics when compared with representative existing techniques. These findings indicate that the proposed method is suitable for LTCI processing in practical PAR systems. Future research will focus on extending this method to real-world scenarios, including environments involving strong sea clutter, interference, and multipath propagation.

APPENDIX

To rigorously establish the validity and superiority of the proposed method, a comprehensive theoretical analysis is conducted in this section. The analysis encompasses four key aspects: (1) the Cramér-Rao lower bound (CRLB) for parameter estimation under PAR's sparse slow-time sampling, and (2) the theoretical basis for determining the ANS range. These analyses transform the proposed method from a heuristic algorithm into a theoretically grounded framework.

A. CRLB for Parameter Estimation

To evaluate the efficiency of the proposed parameter estimator, we derive the CRLB for jointly estimating the motion parameters $\boldsymbol{\theta} = [r, v, a]^T$ from the PAR signal model in (4). The CRLB provides a lower bound on the variance of any unbiased estimator, serving as a benchmark for optimality.

The complex-valued baseband signal for a single target in noise is:

$$s(\hat{t}, t_m) = A\cdot\mathrm{sinc}[\pi B(\hat{t}-\tau(t_m))]\cdot\exp(-j2\pi f_c\tau(t_m))+w(\hat{t}, t_m) \tag{26}$$

where A is the complex amplitude (assumed known for simplicity), $\tau(t_m) = 2(r-vt_m-at_m^2)/c$, and $w(\hat{t}, t_m)$ is i.i.d. complex Gaussian noise with variance σ_w^2. The total Fisher information matrix (FIM) $\mathbf{J}(\boldsymbol{\theta})$ is obtained by summing the contributions from all M pulses and all relevant range samples (within the mainlobe of the sinc function). For a high SNR scenario, the dominant information comes from the phase term $\phi(t_m) = -2\pi f_c\tau(t_m)$.

The FIM element $[\mathbf{J}(\boldsymbol{\theta})]_{ij}$ is given by:

$$[\mathbf{J}(\boldsymbol{\theta})]_{ij} = \frac{2|A|^2}{\sigma_w^2}\sum_{m=1}^{M}\frac{\partial\phi(t_m)}{\partial\theta_i}\frac{\partial\phi(t_m)}{\partial\theta_j} \tag{27}$$

where the derivatives are:

$$\begin{aligned}\frac{\partial\phi}{\partial r} &= \frac{4\pi f_c}{c},\\ \frac{\partial\phi}{\partial v} &= \frac{4\pi f_c}{c}t_m,\\ \frac{\partial\phi}{\partial a} &= \frac{4\pi f_c}{c}t_m^2.\end{aligned} \tag{28}$$

The summation over the non-uniform slow-time instants $[p(m)T_r]$ is critical. Defining the slow-time moment sums:

$$S_k = \sum_{m=1}^{M}[p(m)]^k, \quad k = 0, 1, 2, 3, 4, \tag{29}$$

the FIM can be compactly written as:

$$\mathbf{J}(\boldsymbol{\theta}) = \eta\begin{bmatrix}S_0 & S_1 & S_2\\ S_1 & S_2 & S_3\\ S_2 & S_3 & S_4\end{bmatrix} \tag{30}$$

where $\eta = \frac{32\pi^2|A|^2f_c^2}{c^2\sigma_w^2}$. The CRLB matrix is $\mathbf{C}(\theta) = \mathbf{J}^{-1}(\theta)$. The diagonal elements of $\mathbf{C}$ give the lower bounds for the variances of r, v and a:

$$\mathrm{var}(\hat{r}) \geq [\mathbf{C}]_{11}, \mathrm{var}(\hat{v}) \geq [\mathbf{C}]_{22}, \mathrm{var}(\hat{a}) \geq [\mathbf{C}]_{33}. \tag{31}$$

Key Insight: The bounds depend on the slow-time sequence $p(m)$ through the moments S_k. A well-designed $p(m)$ maximizes the moments S_2, S_4, thereby minimizing the CRLB for velocity and acceleration estimation. This formally justifies the use of sparse array configurations in the slow-time domain.

B. Theoretical Basis for ANS Range

Let $V_{\max}$ denote the maximum plausible radial velocity of the target, which can be determined from prior knowledge of the target type (e.g., 300 m/s for commercial aircraft, 700 m/s for fighter jets, or 2000 m/s for ballistic missiles). The true radial velocity v of the target satisfies $|v| \leq V_{\max}$.

According to the velocity decomposition $v = N_{bg}v_b + v_{0g}$, where $|v_{0g}| < v_b/2$, we have:

$$|N_{bg}| = \left|\frac{v - v_{0g}}{v_b}\right| \leq \frac{|v| + |v_{0g}|}{v_b} < \frac{V_{\max}}{v_b} + \frac{1}{2} \tag{32}$$

Since N_{bg} is an integer, it follows that:

$$|N_{bg}| \leq \left\lfloor\frac{V_{\max}}{v_b} + \frac{1}{2}\right\rfloor = \left\lceil\frac{V_{\max}}{v_b}\right\rceil \tag{33}$$

Therefore, taking $N_{\max} = \lceil V_{\max}/v_b\rceil$ guarantees that for all targets with $|v| \leq V_{\max}$, the corresponding ambiguity number N_{bg} lies within the set $\{-N_{\max}, \ldots, N_{\max}\}$.

Completeness: This search range covers all targets whose speed does not exceed $V_{\max}$, with no omission.

Optimality: If a smaller range $N'_{\max} < N_{\max}$ were used, there would exist some $v \in [-V_{\max}, V_{\max}]$ whose corresponding N_{bg} falls outside the range, leading to missed detection. Hence, this range is the minimum integer search range that covers the entire target velocity interval.

REFERENCES

[1] J. Liu, C. Gao, L. Qin, H. Wen, Y. Su, H. Zhu and C. Yu, "Quasi-Monostatic High-Temperature Radar Cross Section Measurement in Near-Field Region," *IEEE Transactions on Instrumentation and Measurement*, vol. 75, pp. 1-11, 2026.

[2] Y. Liu, T. Huang, H. Meng and X. Wang, "Fundamental Limits of HRR Profiling and Velocity Compensation for Stepped-Frequency Waveforms," *IEEE Transactions on Signal Processing*, vol. 62, no. 17, pp. 4490-4504, 2014.

[3] J. Wan and Y. Zhou and L. Zhang and Z. Chen, "A Doppler Ambiguity Tolerated Method for Radar Sensor Maneuvering Target Focusing and Detection," *IEEE Sensors Journal*, vol. 19, no. 16, pp. 6691-6704, 2019.

[4] Z. Liu and X. Wei and X. Li, "Aliasing-Free Moving Target Detection in Random Pulse Repetition Interval Radar Based on Compressed Sensing," *IEEE Sensors Journal*, vol. 13, no. 7, pp. 2523-2534, 2013.

[5] Z. Niu and J. Zheng and T. Su, "Novel motion parameter estimation and coherent integration algorithm for high maneuvering target with jerk motion," *Signal Processing*, vol. 221, pp. 109467, 2024.

[6] W. Zhu and Z. Liu and H. Xu, "Fast coherent integration method for moving target detection with random PRI variation," *Electronics Letters*, vol. 56, no. 1, pp. 41-43, 2020.

[7] J. Pan and Z. Chen and P. Hu and Q. Bao and S. Xu, "Coherent integration method of high-speed target for random PRI and staggered PW radar," *2019 PhotonIcs & Electromagnetics Research Symposium-Spring (PIERS-Spring)*, pp. 1037–1042, 2019.

[8] J. Tian and X. -G. Xia and W. Cui and G. Yang and S. -L. Wu, "A Coherent Integration Method via Radon-NUFrFT for Random PRI Radar," *IEEE Transactions on Aerospace and Electronic Systems*, vol. 53, no. 4, pp. 2101-2109, 2017.

[9] J. Xu and J. Yu and Y.-N. Peng and X.-G. Xia, "Radon-Fourier Transform for Radar Target Detection, I: Generalized Doppler Filter Bank," *IEEE Transactions on Aerospace and Electronic Systems*, vol. 47, no. 2, pp. 1186–1202, 2011.

[10] L. -C. Qian and J. Xu and X.-G. Xia and W.-F. Sun and T. Long and Y.-N. Peng, "Wideband-scaled radon-fourier transform for high-speed radar target detection," *IET Radar, Sonar & Navigation*, vol. 8, no. 5, pp. 501–512, 2014.

[11] J. Xu and J. Yu and Y.-N. Peng and X.-G. Xia and T. Long, "Space–time radon–fourier transform and applications in radar target detection," *IET Radar, Sonar & Navigation*, vol. 6, pp. 846–857, 2012.

[12] P. Huang and G. Liao and Z. Yang and X.-G. Xia and J.-T. Ma and J. Ma, "Long-time coherent integration for weak maneuvering target detection and high-order motion parameter estimation based on keystone transform," *IEEE Transactions on Signal Processing*, vol. 64, no. 15, pp. 4013–4026, 2016.

[13] S. Yuan and T. Wu and M. Mao and G. Mei and X. Wei, "Application research of keystone transform in weak high-speed target detection in low-PRF narrowband Chirp radar," *2008 9th International Conference on Signal Processing, Beijing, China*, pp. 2452-2456, 2008.

[14] R. Perry and R. DiPietro and R. Fante, "Sar imaging of moving targets," *IEEE Transactions on Aerospace and Electronic Systems*, vol. 35, no. 1, pp. 188–200, 1999.

[15] X. Chen and J. Guan and N. Liu and Y. He, "Maneuvering Target Detection via Radon-Fractional Fourier Transform-Based Long-Time Coherent Integration," *IEEE Transactions on Signal Processing*, vol. 62, no. 4, pp. 939-953, 2014.

[16] X. Chen and J. Guan and N. Liu and Y. He, "Detection of a Low Observable Sea-Surface Target With Micromotion via the Radon-Linear Canonical Transform," *IEEE Geoscience and Remote Sensing Letters*, vol. 11, no. 7, pp. 1225-1229, 2014.

[17] X. Li and G. Cui and W. Yi and L. Kong, "Coherent Integration for Maneuvering Target Detection Based on Radon-Lv's Distribution," *IEEE Signal Processing Letters*, vol. 22, no. 9, pp. 1467-1471, 2015.

[18] J. Xu and X.-G. Xia and S.-B. Peng and J. Yu and Y.-N. Peng and L.-C. Qian, "Radar Maneuvering Target Motion Estimation Based on Generalized Radon-Fourier Transform," *IEEE Transactions on Signal Processing*, vol. 60, no. 12, pp. 6190-6201, 2012.

[19] J. Xu and J. Yu and Y. -N. Peng and X. -G. Xia, "Radon-Fourier Transform for Radar Target Detection (II): Blind Speed Sidelobe Suppression," *IEEE Transactions on Aerospace and Electronic Systems*, vol. 47, no. 4, pp. 2473-2489, 2011.

[20] Y. Sun, Q. Liu, Y. Li, Z. Zheng and S. Chang, "Enhanced Detection of Low-Observable Maneuvering Targets Based on FDGRFT and Lévy Golden Sparrow Search Algorithm," *IEEE Transactions on Instrumentation and Measurement*, pp. 1-1, 2025.

[21] X. Li and G. Cui and W. Yi and L. Kong, "Manoeuvring target detection based on keystone transform and Lv's distribution," *IET Radar, Sonar & Navigation*, vol. 10, no. 7, pp. 1234-1242, 2016.

[22] B. Silva and G. Fraidenraich, "Performance Analysis of the Classic and Robust Chinese Remainder Theorems in Pulsed Doppler Radars," *IEEE Transactions on Signal Processing*, vol. 66, no. 18, pp. 4898-4903, 2018.

[23] S. Wang, C. Men, R. Li and T. -S. Yeo, "A Maneuvering Extended Target Tracking IMM Algorithm Based on Second-Order EKF," *IEEE Transactions on Instrumentation and Measurement*, vol. 73, pp. 1-11, 2024.

[24] H. K. Kwok and D. L. Jones, "Improved instantaneous frequency estimation using an adaptive short-time Fourier transform," *IEEE Transactions on Signal Processing*, vol. 48, no. 10, pp. 2964-2972, 2000.

[25] R. Tao and Y. L. Li and Y.Wang, "Short-time fractional Fourier transform and its applications," *IEEE Transactions on Signal Processing*, vol. 58, no. 5, pp. 2568-2580, 2010.

[26] X. Li and Z. Sun and T. S. Yeo and T. Zhang and W. Yi and G. Cui and L. Kong, "STGRFT for Detection of Maneuvering Weak Target With Multiple Motion Models," *IEEE Transactions on Signal Processing*, vol. 67, no. 7, pp. 1902-1917, 2019.

[27] J. Wang and Y. Gao, "PRF agile radar high-speed target detection non-searching method based on virtual echoes," *Digital Signal Processing*, vol. 164, pp. 105223, 2025.

[28] X. Li and G. Cui and W. Yi and L. Kong, "Fast coherent integration for maneuvering target with high-order range migration via TRT-SKT-LVD," *IEEE Transactions on Aerospace and Electronic Systems*, vol. 52, no. 6, pp. 2803-2814, 2016.

[29] P. P. Vaidyanathan and P. Pal, "Sparse Sensing With Co-Prime Samplers and Arrays," *IEEE Transactions on Signal Processing*, vol. 59, no. 2, pp. 573-586, 2011.

[30] P. Pal and P. Vaidyanathan, "Coprime sampling and the MUSIC algorithm," *2011 Digital Signal Processing and Signal Processing Education Meeting (DSP/SPE)*, pp. 289-294, 2011.

[31] S. Qin and Y. D. Zhang and M. G. Amin, "Generalized Coprime Array Configurations for Direction-of-Arrival Estimation," *IEEE Transactions on Signal Processing*, vol. 63, no. 6, pp. 1377-1390, 2015.

[32] J. Tian and W. Cui and S. Wu, "A Novel Method for Parameter Estimation of Space Moving Targets," *IEEE Geoscience and Remote Sensing Letters*, vol. 11, no. 2, pp. 389-393, 2014.